


Picosecond Electric-Field-Induced Switching of Antiferromagnets

Victor Lopez-Dominguez,^{*} Hamid Almasi, and Pedram Khalili Amiri[†]

Department of Electrical Engineering and Computer Science, Northwestern University, 2145 Sheridan Road, Evanston, Illinois 60208, USA

 (Received 6 July 2018; revised manuscript received 29 October 2018; published 7 February 2019)

We propose a method for switching the Néel vector of an antiferromagnetic thin film by the application of an ultrashort electric field pulse. The electric field induces a reorientation of the antiferromagnetic order parameter due to the voltage-induced modification of the magnetic anisotropy. When the electric field pulse is timed to half the oscillation period of the terahertz antiferromagnetic dynamics, it induces a picosecond-timescale reversal of the Néel vector. Importantly, the electric field required to induce this reversal is as small as approximately 100 mV/nm, comparable to fields used for switching of ferromagnetic tunnel junctions in earlier works. This electric field is determined by the anisotropy of the antiferromagnet, while the much larger exchange field determines the frequency of the resulting dynamics (and hence the switching time). Our results indicate the possibility to switch a 50-nm circular antiferromagnetic element with an energy dissipation of 250 aJ in less than 30 ps and in the absence of any current-induced torque. The electric-field-induced switching of the Néel vector opens an alternative route toward energy-efficient and ultrafast magnetic memories and computing devices based on antiferromagnets.

DOI: [10.1103/PhysRevApplied.11.024019](https://doi.org/10.1103/PhysRevApplied.11.024019)

I. INTRODUCTION

Electrical switching of antiferromagnetic (AFM) materials is of great interest for ultrafast and ultralow energy memory device applications, with potential write times approaching a few picoseconds [1–3]. This is due to the fact that the terahertz dynamics of AFMs [4] is dominated by the exchange field, which is several orders of magnitude larger than the effective fields governing the dynamics of ferromagnetic (FM) materials (typically between 1 and 10 GHz) [5–7]. In addition, AFMs have zero net magnetization, which makes them immune to external magnetic fields and opens the possibility to implement high-density arrays without dipole coupling between adjacent devices.

As in the case of their FM counterparts, AFM spintronic memory devices must achieve two requirements: (i) reliable electrical reading of the magnetic state of the AFM (e.g., the Néel order parameter) and (ii) an energy-efficient and low-voltage method to electrically modify the AFM state. This work focuses on the second requirement by proposing a writing method based on the control of the AFM magnetic anisotropy in response to electrical signals.

Electrical writing in AFMs was first achieved experimentally with assistance from FM layers in exchange-biased systems, with a corresponding change of tunneling

resistance as large as 160% (at 4 K) for the case of NiFe/IrMn/MgO/Pt [8]. However, this type of writing still essentially depends on the presence of a FM material in the device [8,9], resulting in the same limitations currently present in FM-based magnetic random-access memory (MRAM). Recently, a purely AFM MRAM device was demonstrated using magnetoelectric Cr₂O₃ [10]. However, it did not rely on resonant (picosecond) switching, which is one of the important value propositions of AFMs in MRAM. Several works have also explored the use of spin-transfer torque (STT) or spin-orbit torque (SOT) to induce switching or oscillations in AFMs [11–15]. However, the current threshold required to induce the AFM dynamics is determined by the exchange field and is, therefore, rather large. For example, current densities as high as approximately 10⁸ A/cm² were reported in theoretical studies on NiO [16]. Here, we propose utilizing electric fields via the interfacial voltage-controlled magnetic anisotropy (VCMA) effect as a more efficient alternative writing mechanism. The structure considered in this work is shown in Fig. 1(a) and consists of a thin AFM film in contact with an oxide layer (such as MgO). Recently, interfacial VCMA has been theoretically predicted [17] in such material systems, and experiments in the case of IrMn have also provided indirect evidence for voltage control of anisotropy [18], again using the above-mentioned spring-exchange effect. The advantage of this approach is that the switching of the AFM occurs by overcoming the anisotropy field, which is much smaller than the

^{*}victor@northwestern.edu

[†]pedram@northwestern.edu

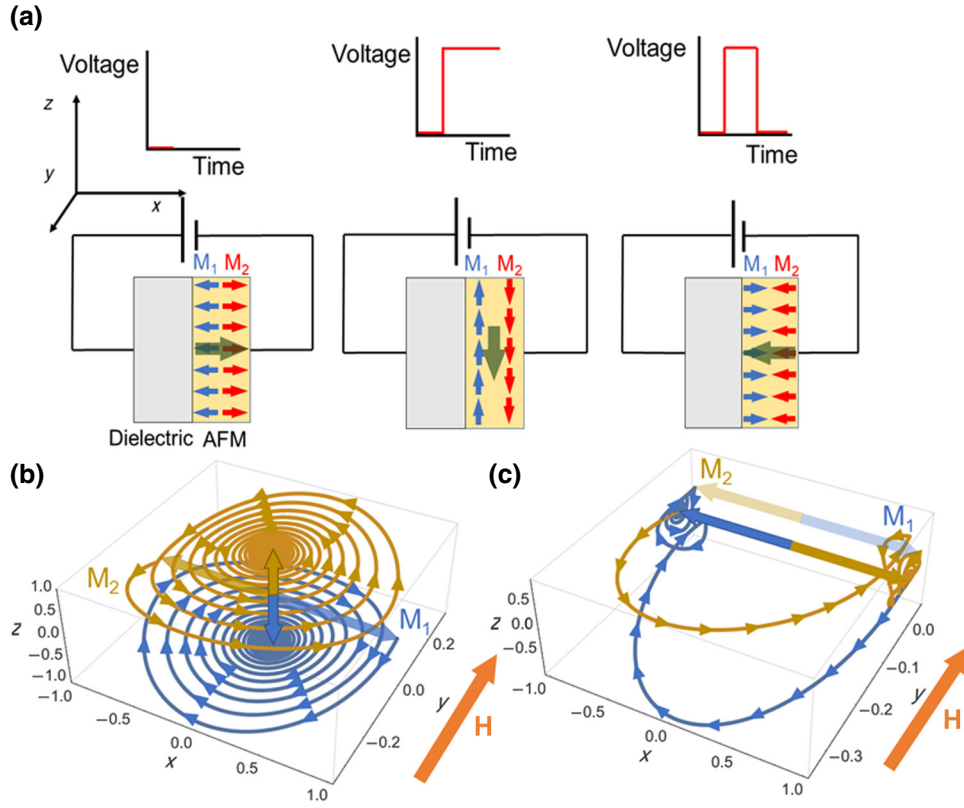


FIG. 1. (a) The device consists of an AFM layer in proximity to a dielectric film. The hybridization of orbitals at the AFM/dielectric interface generates an interfacial perpendicular anisotropy in the AFM layer. The application of a voltage (electric field) changes the easy axis of the AFM, rotating the Néel vector (large green arrow) from the perpendicular to an in-plane direction. If the voltage is pulsed, resonant switching of the Néel vector is accomplished for particular widths of the pulse coinciding with the THz dynamics of the AFM. Notice that the interfaces are oriented in the same direction as the Néel vector is defined in the text, the positive x direction. (b) Simulated trajectory of the two magnetization sublattices, M_1 and M_2 , when a continuous electric field is applied. The anisotropy easy axis and the initial orientation of the two magnetization sublattices are along the x axis, and a 100-Oe bias magnetic field is applied in the positive y direction. (c) Trajectory of the simulated system with the same initial conditions as (b), but applying the electric field during only 21 ps. The initial trajectory of the two sublattices is the same as in (b), but when the electric field is turned off, the sublattice magnetizations are trapped in the new stable positions, which correspond to a 180° reorientation from the original state (inversion of the two magnetization sublattices).

exchange field. As a result, energy-efficient writing is possible without requiring large current densities.

II. MODEL OF ANTIFERROMAGNETIC DYNAMICS

This section presents a dynamical model of the AFM, incorporating the VCMA effect at its interface with the adjacent oxide. The AFM is modeled as two identical macrospin sublattices, which are antiparallel relative to each other and coupled by the exchange interaction [12,16]. Their dynamics are described by two Landau-Lifshitz-Gilbert equations,

$$\frac{d\mathbf{m}_i}{dt} = -\gamma \mathbf{m}_i \times \mathbf{H}_{\text{eff}}^i + \alpha \mathbf{m}_i \times \frac{d\mathbf{m}_i}{dt}, \quad (1)$$

where γ is the gyromagnetic ratio, $\mathbf{H}_{\text{eff}}^i$ is the effective magnetic field at each sublattice ($i = 1, 2$), \mathbf{m}_i is the normalized magnetization, and α corresponds to the damping constant. The effective field is computed from the energy density of the system, obtained for the case of a uniaxial AFM [12],

$$\mathbf{H}_{\text{eff}}^i = -\frac{1}{2} H_{\text{ex}} \mathbf{m}_j + H_{\text{ani}} \mathbf{n}_{\text{ani}} (\mathbf{n}_{\text{ani}} \cdot \mathbf{m}_i) + \mathbf{H} + \mathbf{H}_{\text{th}}, \quad (2)$$

where $\mu_0 H_{\text{ex}} = J/M_s$ and $\mu_0 H_{\text{ani}} = 2K/M_s$ are the exchange and anisotropy fields, respectively, J is the exchange constant, K is the anisotropy constant, M_s is the magnetic saturation, μ_0 is the vacuum permeability, \mathbf{n}_{ani} is the anisotropy easy axis (perpendicular to the interface between the AFM and the oxide), \mathbf{H} is an external bias field, and \mathbf{H}_{th} is a random field to simulate thermal fluctuations. The role of the bias field is to determine the

precession axis of the magnetization sublattices and break the initial symmetry of the system as will be shown in the next sections.

The thermal field is given by

$$\mathbf{H}_{\text{th}} = \sigma \sqrt{\frac{2k_B T \alpha}{\mu_0 \gamma M_s V \Delta t}}, \quad (3)$$

where σ is a random Gaussian vector with zero mean and a standard deviation of 1, k_B is Boltzmann's constant, T is the temperature (300 K during our simulations), V is the volume of the AFM layer (here, we consider a circular device with a radius of 25 nm and a 1-nm thickness), and Δt is the time step chosen during the simulations.

In Eq. (2), the exchange term favors the antiparallel orientation of the sublattices, and the anisotropy term favors their orientation along the easy axis. Note that in Eq. (2), the dipolar and demagnetization fields are not included, which is an approximation justified by the zero-net magnetic moment of the antiferromagnet [19]. The demagnetization field (considering the AFM layer as an ellipsoid in the y - z plane) effectively decreases the perpendicular anisotropy field when the two magnetization sublattices are not perfectly parallel. Therefore, the nonzero magnetic moment during the switching assists the reorientation of the sublattices without qualitatively changing the result.

We assume the effective field contribution due to VCMA to be equal on each sublattice [17]. By analogy to the FM case, the VCMA energy density for each sublattice in an AFM of thickness t in contact with an oxide of thickness d is represented by [20]

$$E_{\text{VCMA}}^i = \frac{\xi V}{dt} [1 - (\mathbf{m}_i \cdot \mathbf{n}_{\text{ani}})^2], \quad (4)$$

where ξ is the VCMA coefficient and V is the applied voltage. From Eq. (4), the effective VCMA field at each sublattice is

$$\begin{aligned} \mathbf{H}_{\text{VCMA}}^i &= V \frac{2\xi}{\mu_0 M_s dt} (\mathbf{m}_i \cdot \mathbf{n}_{\text{ani}}) \cdot \mathbf{n}_{\text{ani}} \\ &= H_{\text{VCMA}} (\mathbf{m}_i \cdot \mathbf{n}_{\text{ani}}) \cdot \mathbf{n}_{\text{ani}}. \end{aligned} \quad (5)$$

Combining Eq. (5) with Eq. (2), the total effective field at each sublattice is

$$\begin{aligned} \mathbf{H}_{\text{eff}}^i &= -\frac{1}{2} H_{\text{ex}} \mathbf{m}_j + H_{\text{ani}} \mathbf{n}_{\text{ani}} (\mathbf{n}_{\text{ani}} \cdot \mathbf{m}_i) \\ &\quad - H_{\text{VCMA}} \mathbf{n}_{\text{ani}} (\mathbf{n}_{\text{ani}} \cdot \mathbf{m}_i) + \mathbf{H} + \mathbf{H}_{\text{th}}. \end{aligned} \quad (6)$$

III. PROPOSED SWITCHING MECHANISM

The device structure and writing mechanism are illustrated in Fig. 1. The sublattice transition from the uniaxial

anisotropy to the in-plane anisotropy in response to a constant (step function) electric field is shown in Figs. 1(a) (middle panel) and 1(b). The resonant switching due to a short (pulse) voltage is depicted in Figs. 1(a) (right panel) and 1(c). For a particular polarity, the applied voltage reduces the effective magnetic anisotropy of the system. For voltages that make the VCMA term in Eq. (6) larger than the anisotropy field, the new stable position for both sublattices is in the plane perpendicular to the original easy axis. This induces the dynamics of the two coupled sublattices, which jointly precess toward this new stable position with a frequency determined by the exchange field. However, the threshold electric field is set by the uniaxial anisotropy of the AFM. This is different from the case of spin currents, where the magnetic switching occurs once the exchange field is overcome by the current-induced stimulus [21]. This decoupling of the threshold switching voltage (determined by anisotropy) from the switching time (determined by exchange) is a key benefit of using VCMA for AFM switching.

To validate the proposed switching mechanism, we numerically solve Eq. (1) using the effective field described by Eq. (6) and adding thermal fluctuations at 300 K (well below the Néel temperature) [20]. The results are described using the Néel and ferromagnetic vectors, defined as $\mathbf{l} = (\mathbf{m}_1 - \mathbf{m}_2)/2$ and $\mathbf{m} = (\mathbf{m}_1 + \mathbf{m}_2)/2$, respectively, in addition to the sublattice magnetizations. The material parameters are similar to previous studies on metallic AFMs, specifically FeMn and FeRh [17,19]. The magnetic saturation is $M_s = 5.66 \times 10^5$ A/m (0.7 T) and the interfacial anisotropy energy density is 0.03 erg/cm², extracted from the predicted value from first principles calculations in reference [17], which in the case of a 1-nm AFM thickness, corresponds to an anisotropy field of 0.1 T. The exchange constant is $J = 3.97$ MJ/m³, corresponding to an exchange field of 7 T. This value is lower than for AFM oxides such as NiO, where the exchange field can be as high as approximately 1000 T [22,23]. To the best of our knowledge, the exchange constant for FeMn has not been measured to date, hence we consider the value for bulk Fe, similar to reference [19]. The VCMA coefficient is the predicted value from first principles calculations [17] in FeRh/MgO ($\xi = 300$ fJ/Vm). The damping constant used during the simulations is 0.02, similar to previous works for metallic AFMs such as FeMn [19]. Finally, the time step used during the simulations with the above described parameters is 10^{-3} ps.

IV. RESULTS AND DISCUSSION

In all simulations, the initial anisotropy is along the x axis [i.e., perpendicular to the AFM-dielectric interface in Fig. 1(a)], so that the y - z plane is the hard plane at zero applied electric field. The sublattices are antiparallel, leading to a zero FM vector. The minimum electric

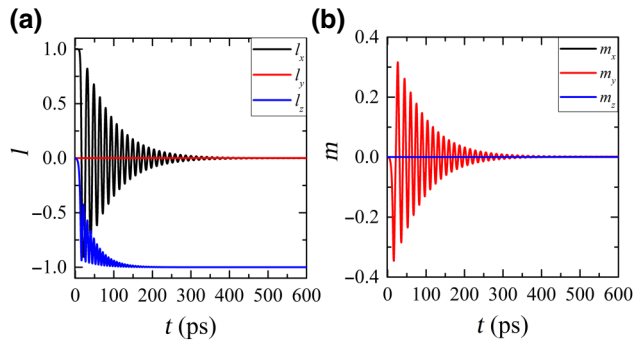


FIG. 2. Time evolution of the three components of the (a) Néel and (b) FM vector for a continuous (i.e., step) electric field of 1 V/nm and an applied bias magnetic field of 100 Oe. The initial easy axis is along the x axis. After applying the electric field, the Néel vector rotates to the z axis (on the new easy anisotropy plane). A small component of the ferromagnetic vector is present during the rotation of the Néel vector, induced by the application of the magnetic field in the y direction and the oscillations of the two magnetization sublattices. When the Néel vector is fully switched from the x axis to the z axis, the ferromagnetic vector value is restored to zero.

field to switch the Néel vector is given by the condition $H_{\text{VCMA}} = H_{\text{ani}}$, and is 100 mV/nm.

We first investigate the reorientation of the Néel vector from out-of-plane to in-plane, as illustrated in Fig. 1(b), due to the application of a continuous electric field. Figures 2(a) and 2(b) show the time evolution of the Néel and FM vector components, respectively, while a constant magnetic field of 100 Oe (along the y direction) and a continuous electric field of 1 V/nm ($H_{\text{VCMA}} = 10H_{\text{ani}}$ starting the Néel vector at $t=0$, along the x axis) are applied to the device. The role of the bias magnetic field is to determine a stable precession axis for the magnetization sublattices as well as helping to start the dynamics once the anisotropy energy is reconfigured by the electric field by inducing a small angle between the sublattices. The bias field can be built into a real device using an in-plane magnetic fixed layer.

The Néel vector reorients from the initial stable position (along the x axis) toward the new equilibrium position in the y - z plane because of the anisotropy reconfiguration. Note that the new equilibrium position of the Néel vector along the z axis is perpendicular to the applied magnetic field. This is consistent with the condition that the Néel and FM vectors are always mutually perpendicular. Complete oscillation of the Néel and FM vectors occurs in periods of approximately 17 ps.

Next, we examine the switching of the Néel vector by a voltage pulse timed to the first half precession of the Néel vector. The initial and final states of the sublattice magnetizations for this case are depicted in Figs. 1(a) and 1(c), respectively, corresponding to the Néel vector switching by 180° along the x axis. Simulation results are plotted in

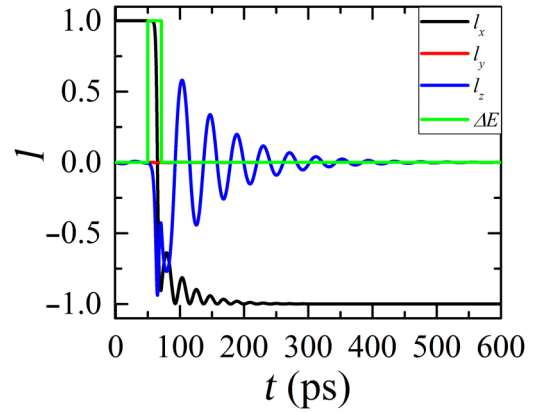


FIG. 3. Switching of the Néel vector with an applied electric field pulse of 1 V/nm, with a pulse width of 21 ps at a constant bias magnetic field of 100 Oe. The Néel vector makes a half oscillation during the application of the pulse. There is an incubation time from the application of the electric field pulse to the initial rotation of the Néel vector.

Fig. 3 for an electric field pulse width of 21 ps, confirming the 180° reorientation of the Néel vector. Note that there is a delay between the application of the pulse and the initial rotation of the Néel vector. This incubation time is defined as the time where the x component of the Néel vector (l_x) drops by 2% from its initial value, increasing the total switching time. The minimum pulse width for switching the Néel vector is, in fact, the sum of this incubation time and the first oscillation half period. In the example shown in Fig. 3, the incubation time is approximately 10 ps.

To better understand the origin of the incubation time, we perform switching simulations at different bias magnetic fields and pulse electric field amplitudes. The results, shown in Fig. 4(a), indicate that at a constant electric field of 1 V/nm, the incubation time reduces from approximately 24 to 7 ps when the magnetic field is increased from 0 to 600 Oe. On the other hand, at a constant magnetic field [100 Oe in Fig. 4(b)], increasing the electric field

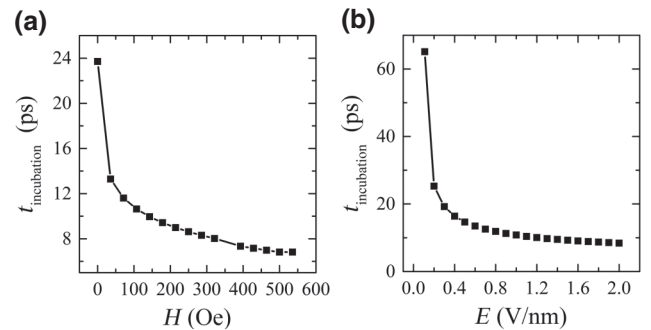


FIG. 4. Incubation time as a function of (a) applied magnetic field at a constant electric field of 1 V/nm, and (b) the applied electric field for a 100-Oe constant bias magnetic field.

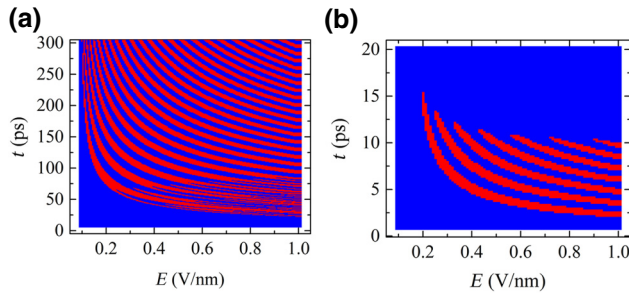


FIG. 5. Switching phase diagram at a constant field of 100 Oe for different electric field pulse times and amplitudes. Two cases are considered with the same damping ($\alpha = 0.02$), but different exchange fields of (a) 7 T and time step of 10^{-3} ps and (b) 1000 T and a time step of 10^{-5} ps. Red corresponds to successful switching and blue to no switching.

pulse amplitude reduces the incubation time from approximately 60 ps to less than 10 ps. Consequently, an increase of the effective magnetic field (either by way of the applied bias or the VCMA field) reduces the incubation time. Even though the physical principle of switching is different in our case, this result is reminiscent of Néel vector switching in AFMs by STT, in which the switching time is reduced for larger currents and magnetic fields [23]. In the proposed mechanism, when the electric field is applied, the initial state of the Néel vector becomes unstable. The application of a small torque, as created by the bias field, is sufficient to deviate the two magnetization sublattices from their antiparallel configuration and initiate the dynamics of the AFM toward the new stable position. As the field increases, the deviations in the relative orientation of the sublattices become larger, thus requiring a shorter time to initiate the dynamics.

Finally, we perform additional simulations to understand the role of different AFM exchange constants, which are varied up to 1000 T, corresponding to the prototypical oxide AFM NiO. For the high exchange field case, the time step of the simulation is also varied to 10^{-5} ps to ensure convergence of the solution. We compute the switching phase diagram as a function of the applied electric field and pulse width at a constant applied magnetic field (100 Oe) and for different values of the exchange constant. The diagram is computed by performing a simulation for each pulse condition and subsequently recording the final state of the Néel vector. Increasing the exchange constant decreases the switching time, consistent with the expected switching mechanism. Note that in both cases in Fig. 5, the anisotropy field is the same (0.1 T) and is much lower than the exchange field, confirming that the dynamics of the Néel vector (hence, the switching time) is, in fact, dominated by the exchange field.

V. CONCLUSIONS

In conclusion, VCMA-induced THz dynamics represents a method to achieve ultrafast spintronic devices based on AFMs with low switching voltages that are determined by the AFM anisotropy rather than the exchange field. Simulations indicate effective switching for constant bias magnetic fields below 100 Oe in the studied exchange field range from 7 to 1000 T. For practical device applications in memory and computing, the total switching energy of the VCMA-induced reversal mechanism is an important figure of merit. Considering the structure of Fig. 1, with dielectric and AFM thicknesses of 1 nm and assuming a resistance-area product similar to ferromagnetic VCMA devices [24], one can estimate the switching energy for a 50-nm-circular AFM device to be approximately 250 aJ. This assumes a switching voltage of 1 V, with a total write time of 30 ps [See Fig. 5(a)]. This total energy consists of a capacitive term (CV^2) which is approximately 175 aJ, and an Ohmic dissipation term of approximately 75 aJ. This energy estimation does not take into account the contributions from any peripheral circuit connected to the device for writing and reading purposes. We note that an approximately similar estimate of the switching energy (450 aJ) has also recently been made for AFM switching using an entirely different voltage-controlled mechanism (strain-mediated magnetoelectric coupling) [19]. The projected switching energy of 250 aJ is more than $20\times$ smaller than the lowest VCMA-induced switching energy reported for FM devices to date [24], pointing to the potential for realizing ultralow-power and ultrafast AFM-based VCMA memory devices.

ACKNOWLEDGMENTS

The authors would like to thank Prof. Nicholas Kioussis and Dr. Farzad Mahfouzi for helpful discussions.

- [1] F. Keffer and C. Kittel, Theory of antiferromagnetic resonance, *Phys. Rev.* **85**, 329 (1952).
- [2] H. Kondoh, Antiferromagnetic resonance in NiO in far-infrared region, *J. Phys. Soc. Jpn.* **15**, 1970 (1960).
- [3] A. B. Shick, S. Khmelevskiy, O. N. Mryasov, J. Wunderlich, and T. Jungwirth, Spin-orbit coupling induced anisotropy effects in bimetallic antiferromagnets: A route towards antiferromagnetic spintronics, *Phys. Rev. B* **81**, 212409 (2010).
- [4] G. Ju, J. Hohlfeld, B. Bergman, R. J. M. van de Veerdonk, O. N. Mryasov, J.-Y. Kim, X. Wu, D. Weller, and B. Koopmans, Ultrafast Generation of Ferromagnetic Order via a Laser-Induced Phase Transformation in FeRh Thin Films, *Phys. Rev. Lett.* **93**, 197403 (2004).
- [5] X. Fan, R. Cao, T. Moriyama, W. Wang, H. W. Zhang, and J. Q. Xiao, Magnetic tunnel junction based microwave detector, *Appl. Phys. Lett.* **95**, 122501 (2009).

- [6] C. Kittel, On the theory of ferromagnetic resonance absorption, *Phys. Rev.* **73**, 155 (1948).
- [7] J. Zhu, J. A. Katine, G. E. Rowlands, Y.-J. Chen, Z. Duan, J. G. Alzate, P. Upadhyaya, J. Langer, P. K. Amiri, K. L. Wang, and I. N. Krivorotov, Voltage-Induced Ferromagnetic Resonance in Magnetic Tunnel Junctions, *Phys. Rev. Lett.* **108**, 197203 (2012).
- [8] B. G. Park, J. Wunderlich, X. Martí, V. Holý, Y. Kurosaki, M. Yamada, H. Yamamoto, A. Nishide, J. Hayakawa, H. Takahashi, A. B. Shick, and T. Jungwirth, A spin-valve-like magnetoresistance of an antiferromagnet-based tunnel junction, *Nat. Mater.* **10**, 347 (2011).
- [9] Y. Y. Wang, C. Song, B. Cui, G. Y. Wang, F. Zeng, and F. Pan, Room-Temperature Perpendicular Exchange Coupling and Tunneling Anisotropic Magnetoresistance in an Antiferromagnet-Based Tunnel Junction, *Phys. Rev. Lett.* **109**, 137201 (2012).
- [10] T. Kosub, M. Kopte, R. Hühne, P. Appel, B. Shields, P. Maletinsky, R. Hübner, M. O. Liedke, J. Fassbender, O. G. Schmidt, and D. Makarov, Purely antiferromagnetic magnetoelectric random access memory, *Nat. Commun.* **8**, 13985 (2017).
- [11] R. Cheng, M. W. Daniels, J.-G. Zhu, and D. Xiao, Ultrafast switching of antiferromagnets via spin-transfer torque, *Phys. Rev. B* **91**, 064423 (2015).
- [12] R. Cheng, D. Xiao, and A. Brataas, Terahertz Antiferromagnetic Spin Hall Nano-Oscillator, *Phys. Rev. Lett.* **116**, 207603 (2016).
- [13] J. Finley and L. Liu, Spin-Orbit-Torque Efficiency in Compensated Ferrimagnetic Cobalt-Terbium Alloys, *Phys. Rev. Appl.* **6**, 054001 (2016).
- [14] K. Olejník, T. Seifert, Z. Kašpar, V. Novák, P. Wadley, R. P. Champion, M. Baumgartner, P. Gambardella, P. Němec, J. Wunderlich, J. Sinova, P. Kužel, M. Müller, T. Kampfrath, and T. Jungwirth, Terahertz electrical writing speed in an antiferromagnetic memory, *Sci. Adv.* **4**, eaar3566 (2018).
- [15] P. Wadley, et al., Electrical switching of an antiferromagnet, *Science* **351**, 587 (2016).
- [16] R. Khymyn, I. Lisenkov, V. Tiberkevich, B. A. Ivanov, and A. Slavin, Antiferromagnetic THz-frequency Josephson-like oscillator driven by spin current, *Sci. Rep.* **7**, 43705 (2017).
- [17] G. Zheng, S.-H. Ke, M. Miao, J. Kim, R. Ramesh, and N. Kioussis, Electric field control of magnetization direction across the antiferromagnetic to ferromagnetic transition, *Sci. Rep.* **7**, 5366 (2017).
- [18] Y. Wang, X. Zhou, C. Song, Y. Yan, S. Zhou, G. Wang, C. Chen, F. Zeng, and F. Pan, Electrical control of the exchange spring in antiferromagnetic metals, *Adv. Mater.* **27**, 3196 (2015).
- [19] A. Barra, J. Domann, K. W. Kim, and G. Carman, Voltage Control of Antiferromagnetic Phases at Near-Terahertz Frequencies, *Phys. Rev. Appl.* **9**, 034017 (2018).
- [20] H. Lee, A. Lee, S. Wang, F. Ebrahimi, P. Gupta, P. Khalili Amiri, and K. L. Wang, Analysis and compact modeling of magnetic tunnel junctions utilizing voltage-controlled magnetic anisotropy, *IEEE Trans. Magn.* **54**, 4400209 (2018).
- [21] T. Jungwirth, X. Marti, P. Wadley, and J. Wunderlich, Antiferromagnetic spintronics, *Nat. Nanotechnol.* **11**, 231 (2016).
- [22] E. V. Gomonay and V. M. Loktev, Spintronics of antiferromagnetic systems (Review Article), *Low Temp. Phys.* **40**, 17 (2014).
- [23] H. V. Gomonay and V. M. Loktev, Spin transfer and current-induced switching in antiferromagnets, *Phys. Rev. B* **81**, 144427 (2010).
- [24] C. Grezes, F. Ebrahimi, J. G. Alzate, X. Cai, J. A. Katine, J. Langer, B. Ocker, P. K. Amiri, and K. L. Wang, Ultra-low switching energy and scaling in electric-field-controlled nanoscale magnetic tunnel junctions with high resistance-area product, *Appl. Phys. Lett.* **108**, 012403 (2016).